

Atmospheric Neutrino Oscillations and New Physics

M.C. Gonzalez-Garcia*

*C.N. Yang Institute for Theoretical Physics,
SUNY at Stony Brook, Stony Brook, NY 11794-3840, USA
IFIC, Universitat de València - C.S.I.C.,
Apt 22085, E-46071 València, Spain*

Michele Maltoni†

*C.N. Yang Institute for Theoretical Physics,
SUNY at Stony Brook, Stony Brook, NY 11794-3840, USA*

Abstract

We study the robustness of the determination of the neutrino masses and mixing from the analysis of atmospheric and K2K data under the presence of different forms of phenomenologically allowed new physics in the ν_μ - ν_τ sector. We focus on vector and tensor-like new physics interactions which allow us to treat, in a model independent way, effects due to the violation of the equivalence principle, violations of the Lorentz invariance both CPT conserving and CPT violating, non-universal couplings to a torsion field and non-standard neutrino interactions with matter. We perform a global analysis of the full atmospheric data from SKI together with long baseline K2K data in the presence of $\nu_\mu \rightarrow \nu_\tau$ transitions driven by neutrino masses and mixing together with sub-dominant effects due to these forms of new physics. We show that within the present degree of experimental precision, the extracted values of masses and mixing are robust under those effects and we derive the upper bounds on the possible strength of these new interactions in the ν_μ - ν_τ sector.

*Electronic address: concha@insti.physics.sunysb.edu

†Electronic address: maltoni@insti.physics.sunysb.edu

I. INTRODUCTION

Neutrino oscillations are entering a new era in which the observations from underground experiments obtained with neutrino beams provided to us by Nature – either from the Sun or from the interactions of cosmic rays in the upper atmosphere – are being confirmed by experiments using “man-made” neutrinos from accelerators and nuclear reactors [1].

For atmospheric neutrinos, Super-Kamiokande (SK) high statistics data [2, 3] established beyond doubt that the observed deficit in the μ -like atmospheric events is due to the neutrinos arriving in the detector at large zenith angles, and it is best explained by ν_μ oscillations. This evidence was also confirmed by other atmospheric experiments such as MACRO [4] and Soudan 2 [5].

The KEK to Kamioka long-baseline neutrino oscillation experiment (K2K) uses an accelerator-produced neutrino beam mostly consisting of ν_μ with a mean energy of 1.3 GeV and a neutrino flight distance of 250 km to probe the same oscillations that were explored with atmospheric neutrinos. Their results [6] show that both the number of observed neutrino events and the observed energy spectrum are consistent with neutrino oscillations, with oscillation parameters consistent with the ones suggested by atmospheric neutrinos.

Oscillations are not the only possible mechanism for atmospheric $\nu_\mu \rightarrow \nu_\tau$ flavour transitions. They can also be generated by a variety of forms of nonstandard neutrino interactions or properties. In general these alternative mechanisms share a common feature: they require the existence of an interaction (other than the neutrino mass terms) that can mix neutrino flavours [7]. Among others this effect can arise due to violations of the equivalence principle (VEP) [8, 9, 10], non-standard neutrino interactions with matter [11], neutrino couplings to space-time torsion fields [12], violations of Lorentz invariance (VLI) [13, 14] and of CPT symmetry [15, 16]. From the point of view of neutrino oscillation phenomenology, the most relevant feature of these scenarios is that, in general, they imply a departure from the E^{-1} energy dependence of the oscillation wavelength [17].

Prior to the highest-statistics SK data, some of these scenarios could provide a good description – alternative to Δm^2 neutrino oscillations – of the atmospheric neutrino phenomenology [18, 19]. However, with more precise data, and in particular with the expansion of the energy range covered by atmospheric neutrino data due to the inclusion of the upward-going muons, these alternative scenarios became disfavoured as leading mechanism to explain the observations [20, 21, 22]. The results from K2K experiment further singled out oscillations as the dominant mechanism of $\nu_\mu \leftrightarrow \nu_\tau$ transitions [23].¹

The question arises, however, to what point the possible presence of these forms of new

¹ Recently [24] SK collaboration has presented a reanalysis of the SK1 data in terms of the reconstructed L/E which allowed them to slightly improve the discrimination between oscillations and alternative mechanisms. Unfortunately, to reproduce such analysis for the subdominant effects discussed here is not possible outside the collaboration.

physics, even if sub-dominant, may affect the derived ranges of masses and mixing from the oscillation analysis of the atmospheric and K2K data. Or in other words, to what level our present determination of the neutrino masses and mixing is robust under the presence of phenomenologically allowed new physics effects.

In this paper we address this question by performing a global analysis of the atmospheric and K2K data with $\nu_\mu \rightarrow \nu_\tau$ transitions driven by neutrino masses and mixing in the presence of some generic forms of new physics. In particular we consider new physics interactions which are vector-like, or tensor-like (scalar interactions cannot be distinguish from oscillations). This allow us to treat, in a model independent way, effects due to the violation of the equivalence principle, violations of the Lorentz invariance both CPT conserving and CPT violating, non-universal couplings to a torsion field and non-standard neutrino interactions in matter. In Sec. II we present the formalism adopted and the data set used. In Sec. III we show the results of our analysis. Conclusions are given in Sec. IV. The technical details of our new statistical analysis of the atmospheric data are described in the appendix.

II. FORMALISM

In what follows we consider some new physics (NP) scenarios which induce new sources of lepton flavour mixing in addition to the “standard” Δm^2 oscillations (Δm^2 -OSC). We concentrate on flavour mixing mechanisms for which the propagation of neutrinos (+) and antineutrinos (−) is governed by the following Hamiltonian [16]:

$$\mathbf{H}_\pm \equiv \frac{\Delta m^2}{4E} \mathbf{U}_\theta \begin{pmatrix} -1 & 0 \\ 0 & 1 \end{pmatrix} \mathbf{U}_\theta^\dagger + \sum_n \sigma_n^\pm \frac{\Delta \delta_n E^n}{2} \mathbf{U}_{\xi_n, \pm \eta_n} \begin{pmatrix} -1 & 0 \\ 0 & 1 \end{pmatrix} \mathbf{U}_{\xi_n, \pm \eta_n}^\dagger, \quad (1)$$

where Δm^2 is the mass-squared difference between the two neutrino mass eigenstates, σ_n^\pm accounts for a possible relative sign of the NP effects between neutrinos and antineutrinos and $\Delta \delta_n$ parametrizes the size of the NP terms. The matrices \mathbf{U}_θ and $\mathbf{U}_{\xi_n, \pm \eta_n}$ are given by:

$$\mathbf{U}_\theta = \begin{pmatrix} \cos \theta & \sin \theta \\ -\sin \theta & \cos \theta \end{pmatrix}, \quad \mathbf{U}_{\xi_n, \pm \eta_n} = \begin{pmatrix} \cos \xi_n & \sin \xi_n e^{\pm i \eta_n} \\ -\sin \xi_n e^{\mp i \eta_n} & \cos \xi_n \end{pmatrix}, \quad (2)$$

where we have also accounted for possible non-vanishing relative phases η_n . For concreteness we will focus on NP effects which are induced by tensor-like and vector-like interactions.

We denote by tensor-like interactions those with $n = 1$ leading to a contribution to the oscillation wavelength which grows linearly with the neutrino energy. For example, Eq. (1) can describe the evolution of ν_μ and ν_τ ’s of different masses in the presence of violation of the equivalence principle (VEP) due to non universal coupling of the neutrinos, $\gamma_1 \neq \gamma_2$ (ν_1 and ν_2 being related to ν_μ and ν_τ by a rotation θ_G), to the local gravitational potential

ϕ [8, 9].² Phenomenology of neutrino oscillations induced or modified by VEP has been widely studied in the literature [25].

In this case

$$\Delta\delta_1 = 2|\phi|(\gamma_1 - \gamma_2) \equiv 2|\phi|\Delta\gamma, \quad \xi_1 = \theta_G, \quad \sigma_1^+ = \sigma_1^-. \quad (3)$$

For constant potential ϕ , this mechanism is phenomenologically equivalent to the breakdown of Lorentz invariance induced by different asymptotic values of the velocity of the neutrinos, $v_1 \neq v_2$, with ν_1 and ν_2 being related to ν_μ and ν_τ by a rotation θ_v [13, 14]. In this case

$$\Delta\delta_1 = (v_1 - v_2)\delta v, \quad \xi_1 = \theta_v, \quad \sigma_1^+ = \sigma_1^-. \quad (4)$$

We denote by vector-like interactions those with $n = 0$ which induce an energy independent contribution to the oscillation wavelength. This may arise, for instance, from a non-universal coupling of the neutrinos, $k_1 \neq k_2$ (ν_1 and ν_2 being related to the ν_μ and ν_τ by a rotation θ_Q), to a space-time torsion field Q [12], so

$$\Delta\delta_0 = Q(k_1 - k_2) \equiv Q\delta k, \quad \xi_0 = \theta_Q, \quad \sigma_0^+ = \sigma_0^-. \quad (5)$$

Violation of CPT due to Lorentz-violating effects also lead to an energy independent contribution to the oscillation wavelength [15, 16] with

$$\Delta\delta_0 = b_1 - b_2 \equiv \delta b, \quad \xi_0 = \theta_{\text{CPT}}, \quad \sigma_0^+ = -\sigma_0^- \quad (6)$$

where b_i are the eigenvalues of the Lorentz violating CPT-odd operator $\bar{\nu}_L^\alpha b_\mu^{\alpha\beta} \gamma_\mu \nu_L^\beta$ and θ_v is the rotation angle between the corresponding neutrino eigenstates and the flavour eigenstates [16].

In all these scenarios, if the NP strength is constant along the neutrino trajectory, the expression of $P_{\nu_\mu \rightarrow \nu_\mu}$ takes the form [16]:

$$P_{\nu_\mu \rightarrow \nu_\mu} = 1 - P_{\nu_\mu \rightarrow \nu_\tau} = 1 - \sin^2 2\Theta \sin^2 \left(\frac{\Delta m^2 L}{4E} \mathcal{R} \right). \quad (7)$$

where the correction to the Δm^2 -OSC wavelength, \mathcal{R} , and to the global mixing angle, Θ , verify

$$\mathcal{R} \cos 2\Theta = \cos 2\theta + \sum_n R_n \cos 2\xi_n, \quad (8)$$

$$\mathcal{R} \sin 2\Theta = |\sin 2\theta + \sum_n R_n \sin 2\xi_n e^{i\eta_n}|, \quad (9)$$

² VEP for massive neutrinos due to quantum effects discussed in Ref. [10] can also be parametrized as Eq. (1) with $n = 2$.

with R_n being the ratio between Δm^2 -induced and the NP-induced contributions to the oscillation wavelength

$$R_n = \sigma_n^+ \frac{\Delta \delta_n E^n}{2} \frac{4E}{\Delta m^2}. \quad (10)$$

For $P_{\bar{\nu}_\mu \rightarrow \bar{\nu}_\mu}$ the same expressions hold with the exchange $\sigma_n^+ \rightarrow \sigma_n^-$ and $\eta_n \rightarrow -\eta_n$.

For the sake of simplicity, in what follows we concentrate in scenarios with one NP source characterized by a unique n . In this case

$$\sin^2 2\Theta = \frac{1}{\mathcal{R}^2} \left(\sin^2 2\theta + R_n^2 \sin^2 2\xi_n + 2R_n \sin 2\theta \sin 2\xi_n \cos \eta_n \right), \quad (11)$$

$$\mathcal{R} = \sqrt{1 + R_n^2 + 2R_n (\cos 2\theta \cos 2\xi_n + \sin 2\theta \sin 2\xi_n \cos \eta_n)}. \quad (12)$$

In Fig. 1 we illustrate the effect of the presence of the NP in the atmospheric neutrino events distributions for Δm^2 -OSC plus sub-dominant CPT-even tensor-like and vector-like NP effects, for some characteristic values of the NP-parameters. In both cases R_n is a growing function of E and the NP effects become relevant in the higher energy samples, in particular for upward going muons.

In order to properly define the intervals of variation of the five parameters Δm^2 , θ , $\Delta \delta_n$, ξ_n , η_n , we can take advantage of the symmetries of the Hamiltonian (see also Ref. [26] for a very similar problem). For a given value of σ_n^+ , from the expressions (1) and (2) we see that the Hamiltonian is invariant under the following transformations:

- $\theta \rightarrow \theta + \pi$,
- $\xi_n \rightarrow \xi_n + \pi$,
- $\eta_n \rightarrow \eta_n + 2\pi$,
- $\Delta m^2 \rightarrow -\Delta m^2$ and $\theta \rightarrow \theta + \pi/2$,
- $\Delta \delta_n \rightarrow -\Delta \delta_n$ and $\xi_n \rightarrow \xi_n + \pi/2$,
- $\xi_n \rightarrow -\xi_n$ and $\eta_n \rightarrow \eta_n + \pi$.

Furthermore, the relevant survival probabilities $P_{\nu_\mu \rightarrow \nu_\mu}$ and $P_{\bar{\nu}_\mu \rightarrow \bar{\nu}_\mu}$ are not affected by a change in the overall sign of the Hamiltonian, as well as change in the global phase of its non-diagonal components. Therefore, we also have:

- $\theta \rightarrow \theta + \pi/2$ and $\xi_n \rightarrow \xi_n + \pi/2$,
- $\theta \rightarrow -\theta$ and $\xi_n \rightarrow -\xi_n$,
- $\eta_n \rightarrow -\eta_n$.

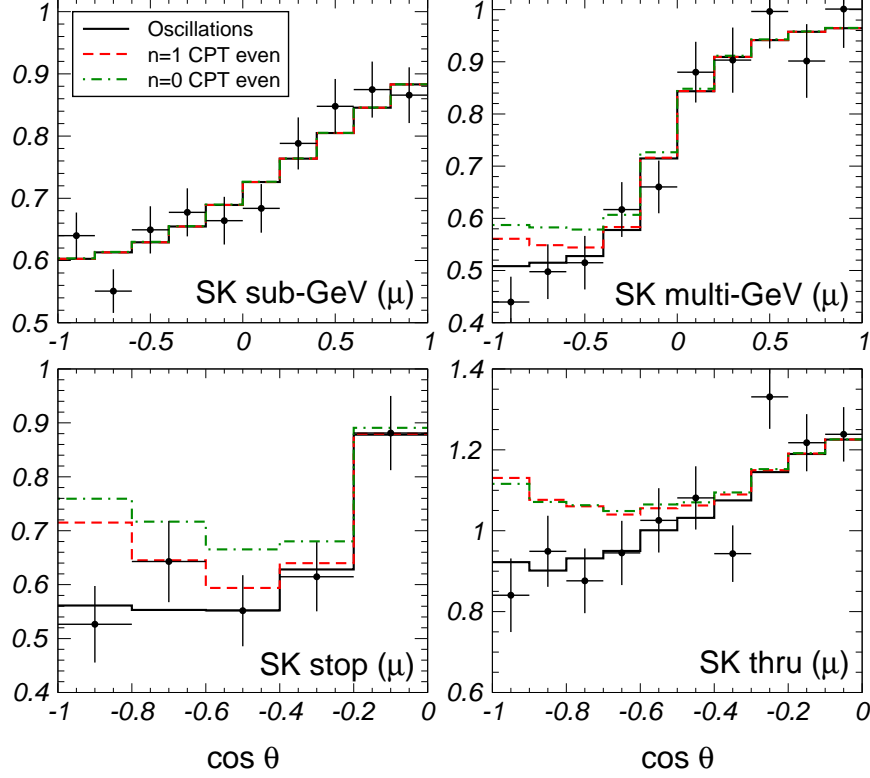


FIG. 1: Zenith-angle distributions (normalized to the no-oscillation prediction) for the Super-Kamiokande μ -like events. The full line gives the distribution for the best fit of Δm^2 -OSC, $\Delta m^2 = 2.2 \times 10^{-3} \text{ eV}^2$ and $\sin^2 \theta = 0.5$. The dashed and dotted lines give the distributions for Δm^2 -OSC+NP scenarios for $n = 1$ and $n = 0$ with $\Delta\delta_1 = 2.0 \times 10^{-24}$ and $\Delta\delta_0 = 4.2 \times 10^{-23} \text{ GeV}$ respectively. In both cases $\eta = \xi = 0$ and the oscillation parameters have been set to their best fit values.

The above set of symmetries allows us to define the ranges of variation of the five parameters as follows:

$$\begin{aligned}
 (a) \quad & \Delta m^2 \geq 0, & (c) \quad & 0 \leq \theta \leq \pi/2, \\
 (b) \quad & \Delta\delta_n \geq 0, & (d) \quad & 0 \leq \xi_n \leq \pi/4, \\
 & & (e) \quad & 0 \leq \eta_n \leq \pi.
 \end{aligned} \tag{13}$$

Thus in the general case we cover the mixing parameter space by using, for instance, $0 \leq \sin^2 \theta \leq 1$ and $0 \leq \sin^2 2\xi_n \leq 1$.

For the case of real relative phase, $\eta_n \in \{0, \pi\}$, one can absorb the two values of η_n into the sign of ξ_n . In this case we drop (e) and replace (d) by:

$$(d') \quad -\pi/4 \leq \xi_n \leq \pi/4 \tag{14}$$

and use instead $-1 \leq \sin 2\xi_n \leq 1$.

Finally we notice that the above derivation is valid for a given sign of σ_n^+ . Keeping the convention of $\Delta m^2 > 0$ and $\Delta \delta_n > 0$ the survival probability for the opposite sign can be obtained by the exchange

$$\sin^2 \theta \rightarrow 1 - \sin^2 \theta \quad \text{and} \quad \eta_n \rightarrow \pi - \eta_n. \quad (15)$$

In addition, we also consider the special case of vector-like NP due to non-standard neutrino-matter interactions (NSI) [11, 19]. In this case the effective Lagrangian describing the evolution of the ν_μ - ν_τ system can be written as [19, 26]

$$\mathbf{H}_\pm = \frac{\Delta m^2}{4E} \mathbf{U}_\theta \begin{pmatrix} -1 & 0 \\ 0 & 1 \end{pmatrix} \mathbf{U}_\theta^\dagger \pm \sqrt{2} G_F N_f(r) \begin{pmatrix} -\varepsilon'_\pm/2 & \varepsilon_\pm \\ \varepsilon_\pm^* & \varepsilon'_\pm/2 \end{pmatrix} \quad (16)$$

where $N_f(r)$ is the number density of the fermion f along the path \vec{r} of the neutrinos propagating in the Earth, and ε_\pm and ε'_\pm parametrize the deviation from standard neutrino interactions: $\sqrt{2} G_F N_f(r) \varepsilon_+$ is the forward scattering amplitude of the FC process $\nu_\mu + f \rightarrow \nu_\tau + f$, and $\sqrt{2} G_F N_f(r) \varepsilon'_+$ is the difference between the $\nu_\tau + f$ and the $\nu_\mu + f$ elastic forward scattering amplitudes. The corresponding amplitudes for antineutrinos are given by ε_- and ε'_- . For simplicity we assume that the interactions for neutrinos and antineutrinos are the same, which implies $\varepsilon'_+ = \varepsilon'_- \equiv \varepsilon'$ and $\varepsilon_+ = \varepsilon_-^* \equiv \varepsilon$. Thus the NSI Hamiltonian contains three real parameters, which can be chosen to be ε' , $|\varepsilon|$ and $\arg(\varepsilon)$. NSI and their interplay with the oscillations have also been studied in different contexts: among others, in relation to supernova neutrinos [27], to the solar neutrino problem [28], to the LSND results oscillation results [29], to neutrinoless double beta decay [30], and to present and future laboratory neutrinos [31].

Formally Eq. (16) can be seen as a special case of Eq. (1) with $n = 0$, $\sigma_0^- = -\sigma_0^+$, and

$$\begin{aligned} \Delta \delta_0 &= 2\sqrt{2} G_F N_f(\vec{r}) \mathcal{F} \equiv 4.58 \times 10^{-22} (2 - Y_p) \frac{\rho(\vec{r})_{\text{Earth}}}{3\text{g/cm}^3} \mathcal{F} \text{ GeV}, \\ \cos(2\xi) &= \frac{\varepsilon'/2}{\mathcal{F}}, \quad \sin(2\xi) = \frac{|\varepsilon|}{\mathcal{F}}, \quad \eta = \arg(\varepsilon), \\ \text{with } \mathcal{F} &= \sqrt{|\varepsilon|^2 + \frac{\varepsilon'^2}{4}}. \end{aligned} \quad (17)$$

Technically the main difference is that NSI only affect the evolution of neutrinos in the Earth, and their strength changes along the neutrino trajectory. Consequently the flavour transition probability cannot be simply read from Eq. (7) and its evaluation requires the numerical solution of the neutrino evolution in the Earth matter. In our calculations we use PREM [33] for the Earth's density profile and a chemical composition with proton/nucleon ratio $Y_p = 0.497$ in the mantle and 0.468 in the core. In what follows for the sake of concreteness we set our normalization on these parameters by considering that the relevant neutrino interaction in the Earth occurs only with down-type quarks.

Concerning the data samples used in the analysis, for atmospheric neutrinos we include in our analysis all the contained events as well as the the upward-going neutrino-induced muon fluxes from the latest 1489 SK data set [2]. This amounts for a total of 55 data points. Details of our new statistical analysis, introduced here for the first time, are presented in the appendix.

For the analysis of K2K we include the data on the normalization and shape of the spectrum of single-ring μ -like events as a function of the reconstructed neutrino energy [6]. We bin the data in five 0.5 GeV bins with $0 < E_{\text{rec}} < 2.5$ GeV plus one bin containing all events above 2.5 GeV. Details of our analysis of the K2K data were presented in Ref. [32] and will not be repeated here. Let us just comment that together with statistical uncertainties we also account for the systematic uncertainties associated with the determination of the neutrino energy spectrum in the near detector, the model dependence of the amount of nQE contamination, the near/far extrapolation and the overall flux normalization.

III. RESULTS AND DISCUSSION

We now describe the results of our χ^2 analysis of the standard Δm^2 -OSC+NP scenarios. As discussed in the previous section the analysis contains five parameters: Δm^2 , θ , $\Delta \delta_n$, ξ_n and η_n (or ε' , $|\varepsilon|$ and $\arg(\varepsilon)$ for NSI). Our results are summarized in Figs. 2, 3, 4 and 5, where we show different projections of the allowed 5-dimensional parameter space.

In Figs. 2 and 3 we plot two-dimensional projections of the allowed parameter region for the analysis of atmospheric and K2K data in presence of $\nu_\mu \rightarrow \nu_\tau$ oscillations and different NP effects parametrized in the form Eq. (1). The corresponding results for the case of NSI are presented in Fig. 3. The regions in each panel are obtained after marginalization of χ^2 with respect to the three undisplayed parameters and they are defined at 90%, 95%, 99% and 3σ CL for 2 d.o.f. ($\Delta\chi^2 = 4.61, 5.99, 9.21$ and 11.83 , respectively).

The left panels in Figs. 2 and 3 show the projection of the allowed region on the oscillation parameters Δm^2 - $\sin^2 \theta$ plane. The best fit point is marked with a star. For the sake of comparison we also show the lines corresponding to the contours of the allowed regions for pure Δm^2 -OSC and mark with a triangle the position of the best fit point. The results are shown for the chosen relative sign $\sigma_n^+ = +1$. For $\sigma_n^+ = -1$ the corresponding region would be obtained by $\sin^2 \theta \rightarrow 1 - \sin^2 \theta$.

The regions on the right panels of Fig. 2 and 3 show the allowed values for the parameters characterizing the strength and mixing of the NP. The full regions correspond to arbitrary values of the relative phase η_n (or equivalently to complex ε parameter for the NSI case) while the lines show the results for real relative phase $\eta_n \in \{0, \pi\}$ (which for NSI corresponds to ε real and either positive or negative, respectively). For this second case we show the allowed region for $-1 \leq \sin 2\xi_n \leq 1$ where for $\sigma_n^+ = +1$ the sector with $-1 \leq \sin 2\xi_n \leq 0$ and $0 \leq \sin 2\xi_n \leq 1$ correspond to $\eta_n = \pi$ and $\eta_n = 0$, respectively, while the opposite

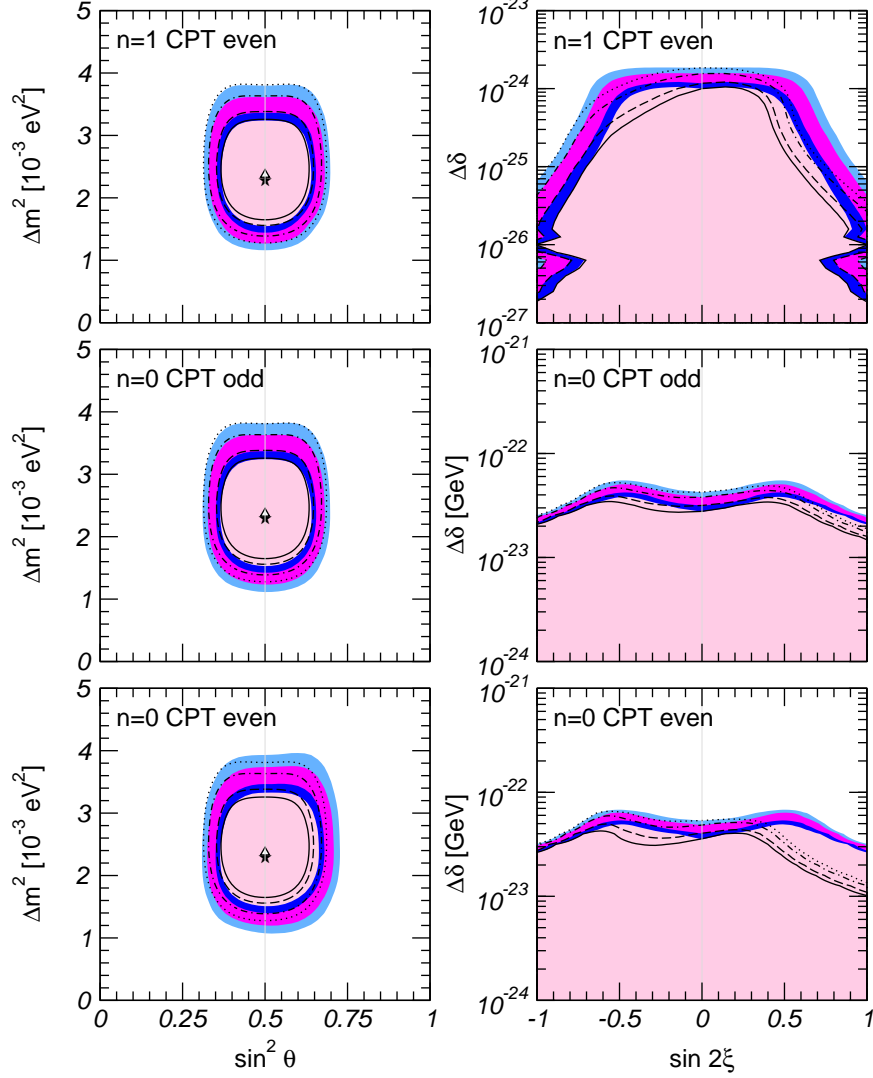


FIG. 2: Allowed parameter regions for the analysis of atmospheric and K2K data in presence of $\nu_\mu \rightarrow \nu_\tau$ oscillations and different NP effects as labeled in the figure. Each panel shows a two-dimensional projection of the allowed five-dimensional region after marginalization with respect to the three undisplayed parameters. The different contours correspond to the two-dimensional allowed regions at 90%, 95%, 99% and 3σ CL. The filled areas in the left panels show the projected two-dimensional allowed region on the oscillation parameters Δm^2 – $\sin^2 \theta$ plane. The best fit point is marked with a star. For the sake of comparison we also show the lines corresponding to the contours in the absence of new physics and mark with a triangle the position of the best fit point. The results are shown for the chosen relative sign $\sigma_n^+ = +1$; for $\sigma_n^+ = -1$ the corresponding region would be obtained by $\sin^2 \theta \rightarrow 1 - \sin^2 \theta$. The regions on the right panels show the allowed values for the parameters characterizing the strength and mixing of the NP. The full regions corresponds to arbitrary values of the phase η_n while the lines correspond to the case $\eta_n \in \{0, \pi\}$.

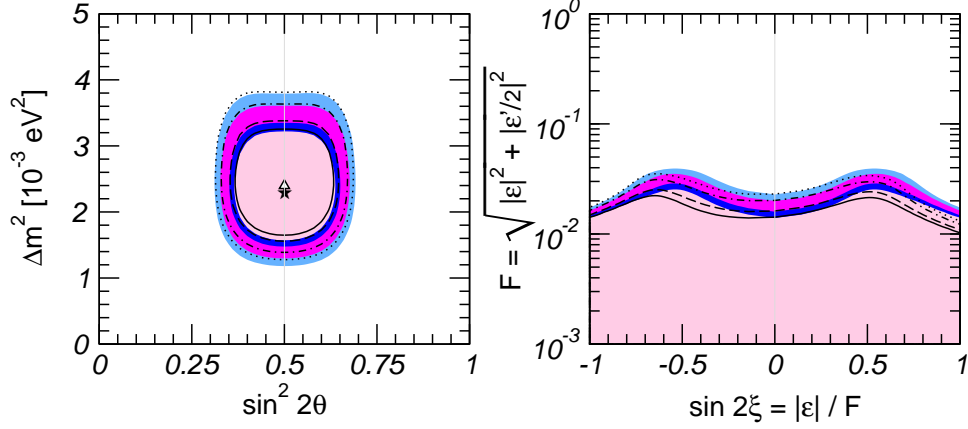


FIG. 3: Same as Fig. 2 for the case of Δm^2 -OSC+NSI.

holds for $\sigma_n^+ = -1$. As discussed in the previous section, for the case of arbitrary phase η_n the full mixing parameter space can be covered by $0 \leq \xi_n \leq \pi/4$, which translates into the symmetry of the allowed region around $\xi_n = 0$.

Several comments are in order. First, from the figures we see that the best fit point for the global Δm^2 -OSC+NP scenarios is always very near the best fit point of pure Δm^2 -OSC

$$\Delta m_{\text{best}}^2 = 2.2 \times 10^{-3} \text{ eV}^2 \quad \sin^2 \theta_{\text{best}} = 0.5. \quad (18)$$

In other words, the data does not show any evidence of presence of NP even as a sub-dominant effect. Second, in agreement with SK analysis [2], we find that with the inclusion of the three-dimensional atmospheric fluxes and improved cross sections as well as with the reanalyzed data points from SK, the best fit point and corresponding allowed regions from the atmospheric+K2K neutrino analysis is shifted to slightly lower values of Δm^2 compared to our previous analysis corresponding to the same data set [32]. Third, the figures illustrate the robustness of the allowed ranges of mass and mixing derived from the analysis of atmospheric and K2K data under the presence of these generic NP effects. Fourth the analysis allow us to derive well-defined upper bounds on the NP strength.

From Fig. 2 we see that the bounds on the NP strength parameter $\Delta \delta_n$ tightens for larger values of ξ_n , being this effect stronger for NP effects leading to sub-dominant oscillations with stronger energy dependence. In particular, for $n = 1$ the bound on $\Delta \delta_n$ for $\sin^2 2\xi_n = 1$ is a factor ~ 50 stronger than that for $\xi_n = 0$, while for $n = 0$ the variation of the bound on $\Delta \delta_n$ with ξ_n is at most a factor ~ 3 . This behaviour can be qualitatively understood by studying the modification of the oscillation probability at the best fit point of oscillations,

$\Delta m_{\text{best}}^2 = 2.2 \times 10^{-3} \text{ eV}^2$ and $\sin^2 2\theta_{\text{best}} = 1$, due to NP effects:

$$\Delta P \equiv \frac{P_{\mu\mu}^{\Delta m^2 + \text{NP}} - P_{\mu\mu}^{\Delta m^2}}{P_{\mu\mu}^{\Delta m^2}} = \tan^2 \phi_b - \frac{1 + 2R_{n,b} \sin 2\xi_n \cos \eta_n + R_{n,b}^2 \sin^2 2\xi_n}{1 + 2R_{n,b} \sin 2\xi_n \cos \eta_n + R_{n,b}^2} \times \frac{\sin^2 \left(\phi_b \sqrt{1 + 2R_{n,b} \sin 2\xi_n \cos \eta_n + R_{n,b}^2} \right)}{1 - \sin^2 \phi_b} \quad (19)$$

where $\phi_b = 2.8 (L/10^3 \text{ km}) (\text{GeV}/E)$ is the Δm^2 oscillation phase at the best fit point and $R_{n,b} = 0.91 \times 10^{21} (\Delta\delta_n/\text{GeV}^{1-n}) (E/\text{GeV})^{n+1}$ is the ratio of NP to the standard oscillation contributions evaluated at the best fit point of oscillations.

From Eq. (19) we find that as long as ϕ_b is small the dependence of ΔP on $R_{n,b}$ (and consequently on $\Delta\delta_n$) is stronger for larger values of $|\sin 2\xi_n|$, which explains the tightening of the bound on $\Delta\delta_n$. This behaviour was found in Ref. [20] for the case with $n = 1$.

However, it is worth noticing that the characteristic value of ϕ_b for which NP effects are relevant depends on n since as n increases the effect becomes important only for higher values of E (see Fig. 1). As a consequence, the characteristic ϕ_b for $n = 0$ is larger than for $n = 1$. Numerical inspection of Eq. (19) also shows that the variation of the dependence of ΔP on $R_{n,b}$ with $\sin 2\xi_n$ decreases as ϕ_b increases. This explains the milder dependence of the bound on $\Delta\delta_n$ with the mixing angle $\sin 2\xi_n$ for $n = 0$ as compared with the $n = 1$ case. The figure also illustrates that imposing that the Hamiltonian is real does not substantially affect these conclusions.

The same arguments apply to the results for NSI in Fig. 3. In particular one sees that, as expected, the results for NSI are very similar to those derived for the $n = 0$ CPT-odd scenario with the identification in Eq. (II), $\langle\Delta\rho_{\text{NSI}}\rangle \sim 7 \times 10^{-22} \mathcal{F} \text{ GeV}$.

More quantitative conclusions on the robustness of the derived ranges for the oscillation parameters and on the bounds on the NP strength can be obtained from Figs. 4 and 5 where we plot the marginalized $\Delta\chi^2$ as a function of the oscillation parameters, Δm^2 and $\sin^2 \theta$, and of the NP strength parameters, for different NP scenarios as labeled in the figures.

In Table I we list the 3σ allowed ranges for Δm^2 and $\sin^2 \theta$. We read that the derived ranges are robust under the presence of these generic forms of NP whose only effect is slightly enlarging the allowed range of Δm^2 by $\lesssim 15\%$, and the lower bound on $\sin^2 2\theta$ by $\lesssim 7\%$ at the 3σ level. We have verified that these conclusions hold for other scenarios characterized by different values of n .

In terms of specific forms of NP the bounds on $\Delta\delta_n$ imply that ATM+K2K limit the possible VLI in the $\nu_\mu\text{--}\nu_\tau$ sector via CPT-even effects to

$$|\delta v| \leq 8.1 \times 10^{-25} (1.6 \times 10^{-24}) \quad (20)$$

and the possible VEP is constrained to

$$|\phi \Delta\gamma| \leq 4.0 \times 10^{-25} (8.0 \times 10^{-25}) \quad (21)$$

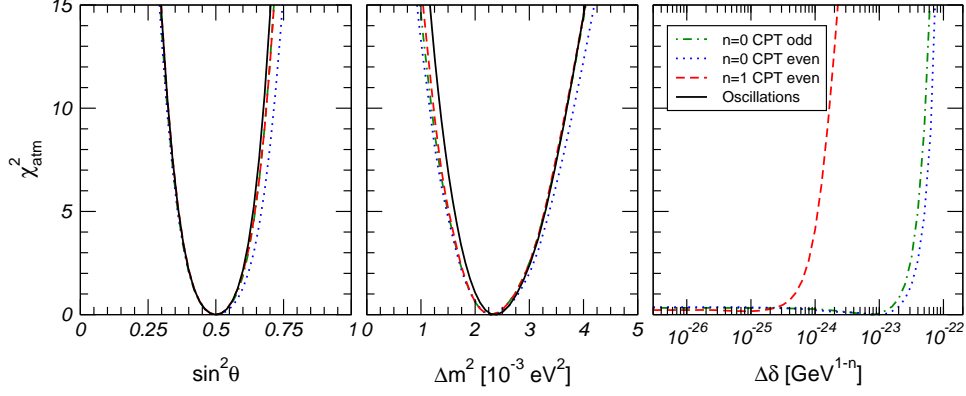


FIG. 4: Dependence of $\Delta\chi^2$ on the oscillation parameters Δm^2 , $\sin^2 \theta$ and on the NP strength parameter $\Delta\delta_n$ for different NP scenarios. The full line corresponds to pure $\nu_\mu \rightarrow \nu_\tau$ Δm^2 -OSC. The dashed, dotted and dot-dashed lines correspond to different Δm^2 -OSC+NP scenarios as labeled in the figure. The figure is shown for $\sigma_n^+ = +1$. As described in the previous section the results hold for $\sigma_n^+ = -1$ with the exchange $\sin^2 \theta \rightarrow 1 - \sin^2 \theta$ (see discussion around Eq. (15)). The individual 3σ bounds in Table I can be read from the corresponding panel with the condition $\Delta\chi^2 \leq 9$.

at 90% (3σ), improving by a factor 8 the previous derived limits in these scenarios [20]. We also find that in the ν_μ - ν_τ the VLI via CP-odd effects is constrained to

$$|\delta b| \leq 3.2 \times 10^{-23} \text{ (} 5.0 \times 10^{-23} \text{) GeV} \quad (22)$$

at 90% (3σ), while non-universality of the neutrino couplings to a torsion field

$$|Q \delta k| \leq 4.0 \times 10^{-23} \text{ (} 6.3 \times 10^{-23} \text{) GeV} \quad (23)$$

at 90% (3σ).

Finally for the case of non-standard neutrino interactions we find the 90% (3σ) bounds

$$\begin{aligned} (-0.021) -0.013 \leq \varepsilon \leq 0.010 \text{ (} 0.017 \text{)} \quad & |\varepsilon'| \leq 0.029 \text{ (} 0.052 \text{)} \quad (\mathbf{H}_{\text{NSI}} \text{ real}), \\ |\varepsilon| \leq 0.013 \text{ (} 0.021 \text{)} \quad & |\varepsilon'| \leq 0.034 \text{ (} 0.060 \text{)} \quad (\mathbf{H}_{\text{NSI}} \text{ complex}) \end{aligned} \quad (24)$$

where the upper limits correspond to the case of real NSI and the lower ones to the general case of complex ε . These limits complement and update the previously derived bounds in Refs. [26, 34].

IV. CONCLUSIONS

In this work we have studied the robustness of our present determination of the neutrino masses and mixing from the analysis of the atmospheric and K2K data under the presence of some new physics effects in the ν_μ - ν_τ sector. In particular, we have performed a global analysis to atmospheric and K2K data for scenarios where vector-like or tensor-like new

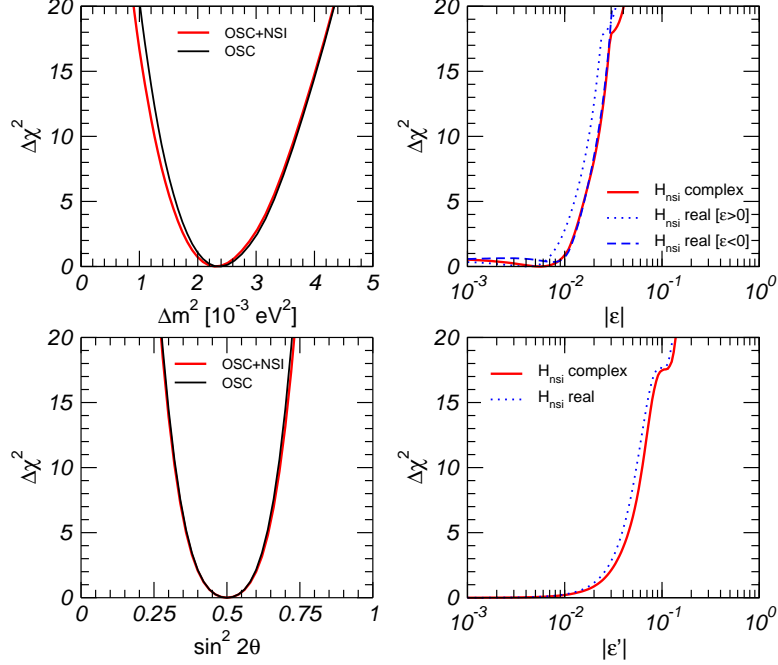


FIG. 5: Dependence of $\Delta\chi^2$ on the oscillation parameters Δm^2 , $\sin^2 \theta$ and on the NP strength parameters for the case of Δm^2 -OSC+NSI.

physics interactions affect the neutrino evolution together with the standard Δm^2 -mixing effect.

We have concluded that the data does not show any evidence of these new physics effects even at the sub-dominant level. As a consequence the derived range of oscillation parameters is robust under the presence of those unknown effects. The quantification of this statement is shown in Figs. 4 and 5 and in Table I, from which we read that inclusion of these new physics effects can at most enlarge the allowed range of Δm^2 by $\lesssim 15\%$ and relax the lower bound on $\sin^2 2\theta$ by $\lesssim 7\%$ at the 3σ level.

From the analysis we have also derived upper bounds on the strength of the new physics effects in the ν_μ - ν_τ sector. In particular we show in Eqs. (20) and (22) the bound on the possible violation of Lorentz Invariance via CPT-even and CPT-odd effects in the neutrino evolution respectively. The constraint on the violation of the equivalence principle (VEP) due to non universal coupling of the neutrinos to gravitational potential is given in Eq. (21), while bounds on non-universal couplings of the neutrino to a torsion field are displayed in Eq. (23). The constraints on non-standard neutrino interactions with matter are shown in Eq. (24).

	Δm^2 -OSC	Δm^2 -OSC+NP			
		$n = 1$ CPT-even	$n = 0$ CPT-even	$n = 0$ CPT-odd	NSI
Δm^2 [10^{-3} eV 2]	1.4–3.6	1.3–3.6	1.2–3.7	1.2–3.6	1.3–3.6
$\sin^2 \theta$	0.33–0.67	0.33–0.68	0.33–0.71	0.33–0.68	0.33–0.67
$\Delta \delta_n$ [GeV $^{n+1}$]	—	$< 1.6 \times 10^{-24}$	$< 6.3 \times 10^{-23}$	$< 5.0 \times 10^{-23}$	$\mathcal{F} \leq 0.035$

TABLE I: Individual 3σ ranges (with 1 d.o.f.) for the oscillation parameters Δm^2 and $\sin^2 \theta$ for the different oscillation plus NP scenarios and 3σ bound on the NP strength parameters. The allowed range of $\sin^2 \theta$ corresponds to $\sigma_n^+ = +1$. For $\sigma_n^+ = -1$ the corresponding range would be obtained by $\sin^2 \theta \rightarrow 1 - \sin^2 \theta$.

Acknowledgments

We are particularly indebted to M. Honda for providing us with their new 3-dimensional atmospheric neutrino fluxes. This work was supported in part by the National Science Foundation grant PHY0098527. MCG-G is also supported by Spanish Grants No FPA-2001-3031 and CTIDIB/2002/24.

APPENDIX A: STATISTICAL TREATMENT OF ATMOSPHERIC DATA

We summarize here our updated statistical analysis of the atmospheric data. For convenience we have adopted the *pull* method used previously by the SK Collaboration (see for instance Refs. [35, 36] for details on their latest analysis) and by the Bari group [23, 37]. There are however some technical differences which we describe next.

The basic idea of the pull method consists in parametrizing the systematic errors and the theoretical uncertainties in terms of a set of variables $\{\xi_i\}$, called *pulls*, which are then treated on the same footing as the other parameters of the model. The χ^2 function can be decomposed into the sum of two parts:

$$\chi^2(\vec{\omega}, \vec{\xi}) = \chi_{\text{data}}^2(\vec{\omega}, \vec{\xi}) + \chi_{\text{pulls}}^2(\vec{\xi}), \quad (\text{A1})$$

where $\vec{\omega}$ denotes the parameters of the model, χ_{data}^2 is the usual term describing the deviation of the experimental results from their theoretical predictions, and the extra term χ_{pulls}^2 provides proper penalties to account for deviations of the systematics and the theoretical inputs from their nominal value. It is convenient to define the pulls in such a way that for each source of systematics or theoretical input i the value $\xi_i = 0$ corresponds to the “expected value” reported by the collaboration or predicted by the theory, and $\xi_i = \pm 1$ corresponds to a 1σ deviation.

For the Super-Kamiokande experiment $\chi_{\text{pulls}}^2(\vec{\xi})$ can be properly written as a positive quadratic function of ξ_i . The interpretations of the pulls is particularly transparent if the

sources of uncertainties are selected to be independent of each other. In this case the pulls are uncorrelated and the expression of χ_{pulls}^2 is very simple:

$$\chi_{\text{pulls}}^2(\vec{\xi}) = \sum_i \xi_i^2. \quad (\text{A2})$$

In its original formulation, the set of pulls selected by Super-Kamiokande [35] did not verify this condition and a correlation matrix between the selected pulls (provided by SK collaboration from their MC simulation) had to be included. In our analysis, however, we have identified the dominant independent sources of systematic uncertainties in SK analysis, and we use them as the basis for our pulls. We have characterized the theoretical and systematic uncertainties in terms of 18 independent sources of error: 4 to parametrize the theoretical uncertainties associated to the atmospheric fluxes (which we describe in Sec. A 1), 6 for the theoretical uncertainties in the interaction cross sections (given in Sec. A 2) and 8 sources of experimental systematic errors (described in Sec. A 3). To the point to which the comparison is possible, this seems close to the approach followed by Super-Kamiokande in their latest analysis [36].

The form of χ_{data}^2 depends on the expected distribution of the experimental results. Under the standard approximation of Gaussian distribution, we have:

$$\chi_{\text{data}}^2(\vec{\omega}, \vec{\xi}) = \sum_n \left(\frac{R_n^{\text{th}}(\vec{\omega}, \vec{\xi}) - R_n^{\text{ex}}}{\sigma_n^{\text{stat}}} \right)^2 \quad (\text{A3})$$

where R_n^{th} (R_n^{ex}) is the ratio between the expected (observed) number of events and the theoretical Monte Carlo for the case of no oscillations. Note that the dependence of χ_{data}^2 on both the parameters $\vec{\omega}$ and the pulls $\vec{\xi}$ is entirely through $R_n^{\text{th}}(\vec{\omega}, \vec{\xi})$. In the pull approach, $\vec{\omega}$ and $\vec{\xi}$ play a very similar role, and in principle should be treated in the same way. However, for the Super-Kamiokande experiment the bounds on $\vec{\xi}$ implied by χ_{pulls}^2 are in general significantly stronger than those implied by χ_{data}^2 , and it is therefore a good approximation to retain the dependence of χ_{data}^2 on $\vec{\xi}$ only to the lowest orders. This is done by expanding $R_n^{\text{th}}(\vec{\omega}, \vec{\xi})$ in powers of ξ_i up to the first order:

$$R_n^{\text{th}}(\vec{\omega}, \vec{\xi}) \approx R_n^{\text{th}}(\vec{\omega}) \left[1 + \sum_{i=1}^{18} \pi_n^i(\vec{\omega}) \xi_i \right], \quad \text{where} \quad \begin{cases} R_n^{\text{th}}(\vec{\omega}) \equiv R_n^{\text{th}}(\vec{\omega}, 0), \\ R_n^{\text{th}}(\vec{\omega}) \pi_n^i(\vec{\omega}) \equiv \left. \frac{\partial R_n^{\text{th}}(\vec{\omega}, \vec{\xi})}{\partial \xi_i} \right|_{\vec{\xi}=0}. \end{cases} \quad (\text{A4})$$

It is easy to prove [37] that under the approximation (A4) Eq. (A1) is mathematically equivalent to the usual covariance definition of the χ^2 which we employed before in Refs. [32, 39]. Thus the small difference in the results are not due to the different statistical treatment, but to differences either in the input parameters or in the updated values used for the systematic and theoretical uncertainties.

Furthermore within the present precision one can safely neglect the dependence of π_n^i on the neutrino parameters $\vec{\omega}$. With this approximation, we can write:

$$\chi^2(\vec{\omega}) = \min_{\vec{\xi}} \left[\sum_{n=1}^{55} \left(\frac{R_n^{\text{th}}(\vec{\omega}) [1 + \sum_i \pi_n^i \xi_i] - R_n^{\text{ex}}}{\sigma_n^{\text{stat}}} \right)^2 + \sum_{i=1}^{18} \xi_i^2 \right] \quad (\text{A5})$$

where we have introduced the function $\chi^2(\vec{\omega}) = \min_{\{\xi_i\}} \chi^2(\vec{\omega}, \vec{\xi})$. It is clear from Eq. (A5) that in the present approach the systematic and theoretical uncertainties are completely characterized by the set of quantities $\{\pi_n^i\}$, which describe the strength of the “coupling” between the pull ξ_i and the observable R_n^{th} .

In the rest of this section we will discuss in detail how we have parametrized and taken into account the various sources of uncertainty and list the derived values for $\{\pi_n^i\}$.

1. Flux uncertainties

Flux uncertainties are theoretical uncertainties arising from our limited knowledge of the atmospheric neutrino fluxes. Following Refs. [35, 36] we have parametrized them in terms of four pulls: $\xi_{\text{norm}}^{\text{flux}}$, $\xi_{\text{tilt}}^{\text{flux}}$, $\xi_{\text{ratio}}^{\text{flux}}$ and $\xi_{\text{zenith}}^{\text{flux}}$. The corresponding coefficients π_n^i are listed in Table II.

- $\xi_{\text{norm}}^{\text{flux}}$ is the pull associated to the total normalization error, which we set to $\sigma_{\text{norm}}^{\text{flux}} = 20\%$ [38].
- $\xi_{\text{tilt}}^{\text{flux}}$ is a “tilt” factor which parametrizes possible deviations of the energy dependence of the atmospheric fluxes from the simple power law. Following Refs. [35, 36], we define:

$$\Phi_\delta(E) = \Phi_0(E) \left(\frac{E}{E_0} \right)^\delta \approx \Phi_0(E) \left[1 + \delta \ln \frac{E}{E_0} \right] \quad (\text{A6})$$

and assume an uncertainty on the factor δ , $\sigma_\delta = 5\%$ [35, 36]. Also in analogy with Refs. [35, 36] we have chosen $E_0 = 2$ GeV. We then calculate numerically the coefficients π_n^{tilt} as follows: we compute the expected number of events for a given bin N_n using $\Phi_\delta(E)$ for the central value of δ and for $\delta \pm \sigma_\delta$ and obtain the corresponding coupling π_n^{tilt} as the relative change in N_n . The results reported in the second column of Table II are obtained neglecting the effect of oscillations. However we have verified that when the dependence of the π_n^{tilt} on the neutrino oscillation parameters is properly taken into account we find very similar results.

- $\xi_{\text{ratio}}^{\text{flux}}$ parametrizes the uncertainty on the ν_μ/ν_e ratio, which is assumed to be $\sigma_{\mu/e} = 5\%$ [35, 36, 38] and following Ref. [35] we assign a coupling $\pi_\mu^{\mu/e} = -\pi_e^{\mu/e} = \sigma_{\mu/e}/2$.
- $\xi_{\text{zenith}}^{\text{flux}}$ describes the uncertainty on the zenith angle dependence, which we assume energy independent. As in Ref. [35] we parametrize the coupling for this pull for the

Sample	Bin	$\xi_{\text{norm}}^{\text{flux}}$	$\xi_{\text{tilt}}^{\text{flux}}$	$\xi_{\text{ratio}}^{\text{flux}}$	$\xi_{\text{zenith}}^{\text{flux}}$
sub-GeV (e, μ)	1	20%	$(-1.44, -1.11) \times 5\%$	$(-2.5\%, +2.5\%)$	$-0.9 \times 5\%$
	2	20%	$(-1.43, -1.11) \times 5\%$	$(-2.5\%, +2.5\%)$	$-0.7 \times 5\%$
	3	20%	$(-1.42, -1.11) \times 5\%$	$(-2.5\%, +2.5\%)$	$-0.5 \times 5\%$
	4	20%	$(-1.42, -1.10) \times 5\%$	$(-2.5\%, +2.5\%)$	$-0.3 \times 5\%$
	5	20%	$(-1.42, -1.10) \times 5\%$	$(-2.5\%, +2.5\%)$	$-0.1 \times 5\%$
	6	20%	$(-1.42, -1.10) \times 5\%$	$(-2.5\%, +2.5\%)$	$+0.1 \times 5\%$
	7	20%	$(-1.42, -1.10) \times 5\%$	$(-2.5\%, +2.5\%)$	$+0.3 \times 5\%$
	8	20%	$(-1.43, -1.10) \times 5\%$	$(-2.5\%, +2.5\%)$	$+0.5 \times 5\%$
	9	20%	$(-1.44, -1.10) \times 5\%$	$(-2.5\%, +2.5\%)$	$+0.7 \times 5\%$
	10	20%	$(-1.46, -1.10) \times 5\%$	$(-2.5\%, +2.5\%)$	$+0.9 \times 5\%$
multi-GeV (e, μ)	1	20%	$(+0.35, +0.91) \times 5\%$	$(-2.5\%, +2.5\%)$	$-0.9 \times 5\%$
	2	20%	$(+0.38, +0.92) \times 5\%$	$(-2.5\%, +2.5\%)$	$-0.7 \times 5\%$
	3	20%	$(+0.42, +0.94) \times 5\%$	$(-2.5\%, +2.5\%)$	$-0.5 \times 5\%$
	4	20%	$(+0.49, +0.98) \times 5\%$	$(-2.5\%, +2.5\%)$	$-0.3 \times 5\%$
	5	20%	$(+0.56, +1.04) \times 5\%$	$(-2.5\%, +2.5\%)$	$-0.1 \times 5\%$
	6	20%	$(+0.56, +1.04) \times 5\%$	$(-2.5\%, +2.5\%)$	$+0.1 \times 5\%$
	7	20%	$(+0.49, +0.98) \times 5\%$	$(-2.5\%, +2.5\%)$	$+0.3 \times 5\%$
	8	20%	$(+0.43, +0.95) \times 5\%$	$(-2.5\%, +2.5\%)$	$+0.5 \times 5\%$
	9	20%	$(+0.39, +0.93) \times 5\%$	$(-2.5\%, +2.5\%)$	$+0.7 \times 5\%$
	10	20%	$(+0.35, +0.90) \times 5\%$	$(-2.5\%, +2.5\%)$	$+0.9 \times 5\%$
stopping μ events	1	20%	$+1.75 \times 5\%$	—	$-0.9 \times 5\%$
	2	20%	$+1.72 \times 5\%$	—	$-0.7 \times 5\%$
	3	20%	$+1.73 \times 5\%$	—	$-0.5 \times 5\%$
	4	20%	$+1.76 \times 5\%$	—	$-0.3 \times 5\%$
	5	20%	$+1.84 \times 5\%$	—	$-0.1 \times 5\%$
thru-going μ events	1	20%	$+4.64 \times 5\%$	—	$-0.95 \times 5\%$
	2	20%	$+4.34 \times 5\%$	—	$-0.85 \times 5\%$
	3	20%	$+4.48 \times 5\%$	—	$-0.75 \times 5\%$
	4	20%	$+4.43 \times 5\%$	—	$-0.65 \times 5\%$
	5	20%	$+4.68 \times 5\%$	—	$-0.55 \times 5\%$
	6	20%	$+4.62 \times 5\%$	—	$-0.45 \times 5\%$
	7	20%	$+4.61 \times 5\%$	—	$-0.35 \times 5\%$
	8	20%	$+4.96 \times 5\%$	—	$-0.25 \times 5\%$
	9	20%	$+5.01 \times 5\%$	—	$-0.15 \times 5\%$
	10	20%	$+5.22 \times 5\%$	—	$-0.05 \times 5\%$

TABLE II: Coupling factors π_n^i of the flux pulls $\xi_{\text{norm}}^{\text{flux}}$, $\xi_{\text{tilt}}^{\text{flux}}$, $\xi_{\text{ratio}}^{\text{flux}}$ and $\xi_{\text{zenith}}^{\text{flux}}$ with the various observables. When the notation (v_1, v_2) is used (second and third column for contained events), the first number refer to e -like events and the second to μ -like events.

Sample	$\xi_{\text{norm}}^{\text{QE}}$	$\xi_{\text{ratio}}^{\text{QE}}$	$\xi_{\text{norm}}^{1\pi}$	$\xi_{\text{ratio}}^{1\pi}$	$\xi_{\text{norm}}^{\text{DIS}}$	$\xi_{\text{ratio}}^{\text{DIS}}$
sub-GeV e	11.3%	-0.19%	3.2%	-0.10%	0.5%	-0.01%
sub-GeV μ	11.3%	+0.19%	3.2%	+0.11%	0.5%	+0.01%
multi-GeV e	6.1%	-0.20%	5.0%	-0.13%	3.9%	-0.49%
multi-GeV μ	2.1%	+0.07%	5.2%	+0.14%	7.7%	+0.98%
stopping μ	2.3%	—	1.4%	—	7.5%	—
thru-going μ	0.5%	—	0.2%	—	9.6%	—

TABLE III: Coupling factors π_n^i of the cross-section pulls $\xi_{\text{norm}}^{\text{QE}}$, $\xi_{\text{ratio}}^{\text{QE}}$, $\xi_{\text{norm}}^{1\pi}$, $\xi_{\text{ratio}}^{1\pi}$, $\xi_{\text{norm}}^{\text{DIS}}$ and $\xi_{\text{ratio}}^{\text{DIS}}$ with the various observables. The couplings are the same for all the bins in a given data sample.

bin n of a given sample as $\pi_n^{\text{zenith}} = 5\% \langle \cos \theta \rangle_n$. This means that this uncertainty can induce an error in the up/down asymmetry of events which we conservatively take to be 5%. In Ref. [35] the assumed up/down uncertainty was smaller (2.5%) and a separate zenith-pull was introduced for the horizontal-to-vertical ratio uncertainty of 2%. We have verified that within the present precision both parametrizations of the uncertainties in the zenith angle distribution give very similar results.

2. Cross-section uncertainties

Cross section uncertainties are theoretical uncertainties associated to our ignorance on the neutrino interaction cross section. In our calculation we follow the standard approach and consider separately the contributions to the interaction cross section from the exclusive channels of lower multiplicity: quasi-elastic scattering (QE), and single pion production (1π), and include all additional channels as part of the deep inelastic (DIS) cross section (also refer to as multi-pion). We neglect for simplicity coherent scattering on oxygen and neutral-current interactions, which contribute only marginally to the considered data samples.

We assume that each of these three contributions to the cross sections are subject to different sources of uncertainties which allow to consider the corresponding pulls as independent. For each type of neutrino interactions we introduce two pulls:

- $\xi_{\text{norm}}^{\text{QE}}$, $\xi_{\text{norm}}^{1\pi}$, $\xi_{\text{norm}}^{\text{DIS}}$ describe the total normalization errors. We conservatively assume $\sigma_{\text{norm}}^{\text{QE}} = 15\%$ and $\sigma_{\text{norm}}^{1\pi} = 15\%$. For the normalization error of the DIS cross section we estimate $\sigma_{\text{norm}}^{\text{DIS}} = 15\%$ for contained events and $\sigma_{\text{norm}}^{\text{DIS}} = 10\%$ for upward-going muons from the spread of theoretical predictions arising from the use of different sets of nucleon structure functions. The relevant coefficients π_n^i are listed in Table III. They are obtained computing the relative change in the number of expected events in a given data sample arising from the use of either σ_i or $\sigma_i \pm \sigma_{\text{norm}}^i$ for each of the three contributions to the cross section.

Sample	$\xi_{\text{hadron}}^{\text{sys}}$	$\xi_{\mu/e}^{\text{sys}}$	$\xi_{\text{ring}}^{\text{sys}}$	$\xi_{\text{f-vol}}^{\text{sys}}$	$\xi_{\text{E-cal}}^{\text{sys}}$	$\xi_{\text{FC/PC}}^{\text{sys}}$	$\xi_{\text{track}}^{\text{sys}}$	$\xi_{\text{up-eff}}^{\text{sys}}$
sub-GeV e	-0.25%	-1.1%	-0.75%	-0.3%	-0.4%	—	—	—
sub-GeV μ	+0.25%	+1.1%	+0.75%	+0.3%	+0.4%	—	—	—
multi-GeV e	-0.50%	-1.6%	-2.75%	-0.5%	-0.4%	—	—	—
multi-GeV μ	+1.10%	+1.6%	+5.40%	+1.4%	+2.0%	2.85%	—	—
stopping μ	—	—	+0.30%	+0.7%	+0.3%	—	6.4%	1.4%
thruoing μ	—	—	+0.30%	+0.7%	+0.3%	—	1.4%	1.0%

TABLE IV: Coupling factors of the systematics pulls $\xi_{\text{hadron}}^{\text{sys}}$, $\xi_{\mu/e}^{\text{sys}}$, $\xi_{\text{ring}}^{\text{sys}}$, $\xi_{\text{f-vol}}^{\text{sys}}$, $\xi_{\text{E-cal}}^{\text{sys}}$, $\xi_{\text{PC-nrm}}^{\text{sys}}$, $\xi_{\text{FC/PC}}^{\text{sys}}$, $\xi_{\text{track}}^{\text{sys}}$ and $\xi_{\text{up-eff}}^{\text{sys}}$ with the various observables. The coefficients are the same for all the bins in a given data sample.

- $\xi_{\text{ratio}}^{\text{QE}}$, $\xi_{\text{ratio}}^{1\pi}$, $\xi_{\text{ratio}}^{\text{DIS}}$ parametrize the uncertainty of the $\sigma_{i,\nu_\mu}/\sigma_{i,\nu_e}$ ratios. This error is relevant only for contained events, and it is much smaller than the total normalization uncertainty. The numbers listed in Table III are obtained from Ref. [35].

3. Systematic uncertainties

The systematics uncertainties of the Super-Kamiokande experiment are derived from Tables 9.2, 9.3, 9.4 and 9.5 of Ref. [35]. We include in our calculations the following sources of systematics:

- $\xi_{\text{hadron}}^{\text{sys}}$ is the pull for the uncertainty associated with the simulation of hadronic interactions;
- $\xi_{\mu/e}^{\text{sys}}$ is the pull for the errors in the particle identification procedure;
- $\xi_{\text{ring}}^{\text{sys}}$ is the pull for the uncertainty coming from the ring-counting procedure;
- $\xi_{\text{f-vol}}^{\text{sys}}$ is the pull for the uncertainty in the fiducial volume determination;
- $\xi_{\text{E-cal}}^{\text{sys}}$ is the pull for the uncertainty in the energy calibration;
- $\xi_{\text{PC-nrm}}^{\text{sys}}$ is the pull for the relative normalization between partially-contained and fully-contained events.
- $\xi_{\text{track}}^{\text{sys}}$ is the pull for the uncertainty in the track reconstruction of upgoing muons;
- $\xi_{\text{up-eff}}^{\text{sys}}$ is the pull for the uncertainty in the detection efficiency of upgoing muons and the stopping-thruoing separation.

[1] For a recent review see M.C. Gonzalez-Garcia and Y. Nir, Rev. Mod. Phys. **75** 345 (2003).

- [2] Y. Hayato, SuperKamiokande Coll., in *International Europhysics Conference on High Energy Physics*, Aachen July 2002, <http://eps200e.phisik.rwth-aachen.de>.
- [3] Y. Fukuda *et al.*, Phys. Lett. **B433**, (1998) 9; Phys. Lett. **B436**, (1998) 33 ; Phys. Lett. **B467**, (1999) 185 ; Phys. Rev. Lett. **82**, (1999) 2644.
- [4] M. Ambrosio *et al.*, MACRO Coll., Phys. Lett. B **517**, (2001) 59.
- [5] D. A. Petyt [Soudan-2 Collaboration], Nucl. Phys. Proc. Suppl. **110**, 349 (2002).
- [6] M. H. Ahn *et al.*, Phys. Rev. Lett. **90**, 041801 (2003)
- [7] For a recent review see, S. Pakvasa and J. W. F. Valle, Proc. Indian Natl. Sci. Acad. **70A**, 189 (2003)
- [8] M. Gasperini, Phys. Rev. D **38** (1988) 2635; Phys. Rev. D **39**, 3606 (1989);
- [9] A. Halprin and C.N. Leung, Phys. Rev. Lett. **67**, 1833 (1991).
- [10] G. Z. Adunas, E. Rodriguez-Milla and D. V. Ahluwalia, Phys. Lett. B **485**, 215 (2000)
- [11] L. Wolfenstein, Phys. Rev. **D17**, 236 (1978)
- [12] V. De Sabbata and M. Gasperini, Nuovo Cimento A **65**, 479 (1981).
- [13] S. Coleman and S.L. Glashow, Phys. Lett. B **405**, 249 (1997).
- [14] S.L. Glashow, A. Halprin, P.I. Krastev, C.N. Leung, and J. Pantaleone, Phys. Rev. D **56**, 2433 (1997).
- [15] D. Colladay and V.A. Kostelecky, *Phys. Rev.* **D55**, 6760 (1997).
- [16] S. Coleman and S.L. Glashow, Phys. Rev. D **59**, 116008 (1999).
- [17] O. Yasuda, in the Proceedings of the Workshop on General Relativity and Gravitation, Tokyo, Japan, 1994, edited by K. Maeda, Y. Eriguchi, T. Futamase, H. Ishihara, Y. Kojima, and S. Yamada (Tokyo University, Japan, 1994), p. 510 (gr-qc/9403023).
- [18] R. Foot, C.N. Leung, and O. Yasuda, Phys. Lett. B **443**, 185 (1998).
- [19] M. C. Gonzalez-Garcia *et al.*, Phys. Rev. Lett. **82**, 3202 (1999)
- [20] G. L. Fogli, E. Lisi, A. Marrone and G. Scioscia, Phys. Rev. D **60**, 053006 (1999)
- [21] P. Lipari and M. Lusignoli, Phys. Rev. D **60** (1999) 013003 [hep-ph/9901350].
- [22] N. Fornengo, M. C. Gonzalez-Garcia and J. W. F. Valle, JHEP **0007** (2000) 006.
- [23] G. L. Fogli, E. Lisi, A. Marrone and D. Montanino, Phys. Rev. D **67**, 093006 (2003)
- [24] Talk by M. Ishitsuka at 5th Workshop on "Neutrino Oscillations and their Origin" (NOON2004), <http://www-sk.icrr.u-tokyo.ac.jp/noon2004/>.
- [25] M.N. Butler, S. Nozawa, R. Malaney, and A.I. Boothroyd, Phys. Rev. D **47**, 2615 (1993); J. Pantaleone, A. Halprin, and C.N. Leung, Phys. Rev. D **47**, 4199 (1993); K. Iida, H. Minakata, and O. Yasuda, Mod. Phys. Lett. A **8**, 1037 (1993); H. Minakata and H. Nunokawa, Phys. Rev. D **51**, 6625 (1995); J.N. Bahcall, P.I. Krastev, and C.N. Leung, Phys. Rev. D **52**, 1770 (1995); A. Halprin, C.N. Leung, and J. Pantaleone, Phys. Rev. D **53**, 5365 (1996); J.R. Mureika and R.B. Mann, Phys. Lett. B **368**, 112 (1996); R.B. Mann and U. Sarkar, Phys. Rev. Lett. **76**, 865 (1996); J.R. Mureika, Phys. Rev. D **56**, 2048 (1997); A. Halprin and C.N. Leung, Phys. Lett. B **416**, 361 (1998); H. Casini, J.C. D'Olivo, R. Montemayor, and L.F. Urrutia, Phys.

- Rev. D **59**, 062001 (1999); S.W. Mansour and T.K. Kuo, Phys. Rev. D **60**, 097301 (2000); A. M. Gago, M. M. Guzzo, P. C. de Holanda, H. Nunokawa, O. L. G. Peres, V. Pleitez and R. Zukanovich Funchal, Phys. Rev. D **65**, 073012 (2002); A. Raychaudhuri and A. Sil, Phys. Rev. D **65**, 073035 (2002); M. M. Guzzo, H. Nunokawa and R. Tomas, Astropart. Phys. **18**, 277 (2002).
- [26] N. Fornengo, M. Maltoni, R. T. Bayo and J. W. F. Valle, Phys. Rev. D **65**, 013010 (2002).
- [27] J. W. F. Valle, Phys. Lett. B **199** (1987) 432; H. Nunokawa, Y. Z. Qian, A. Rossi, and J. W. Valle, Phys. Rev. D **54**, 4356 (1996); H. Nunokawa, A. Rossi, and J. W. Valle, Nucl. Phys. B **482**, 481 (1996); S.W. Mansour and T.K. Kuo, Phys. Rev. D **58**, 013012 (1998); S. Bergmann and A. Kagan, Nucl. Phys. B **538**, 368 (1999). G. L. Fogli, E. Lisi, A. Mirizzi and D. Montanino, Phys. Rev. D **66**, 013009 (2002);
- [28] M. Guzzo, A. Masiero and S. Petcov, Phys. Lett. **B260**, 154 (1991); E. Roulet, Phys. Rev. **D44**, 935 (1991); V. Barger, R. J. N. Phillips and K. Whisnant, Phys. Rev. **D44**, 1629 (1991); S. Bergmann, Nucl. Phys. **B515**, 363 (1998); E. Ma and P. Roy, Phys. Rev. Lett. **80**, 4637 (1998); S. Bergmann, M. M. Guzzo, P. C. de Holanda, P. I. Krastev and H. Nunokawa, Phys. Rev. D **62**, 073001 (2000); M. Guzzo, P. C. de Holanda, M. Maltoni, H. Nunokawa, M. A. Tortola and J. W. F. Valle, Nucl. Phys. B **629**, 479 (2002); A. Friedland, C. Lunardini and C. Pena-Garay, hep-ph/0402266; M. M. Guzzo, P. C. de Holanda and O. L. G. Peres, hep-ph/0403134.
- [29] S. Bergmann and Y. Grossman, Phys. Rev. D **59**, 093005 (1999).
- [30] S. Bergmann, H.V. Klapdor-Kleingrothaus, and H. Päs, Phys. Rev. D **62**, 113002 (2000).
- [31] Y. Grossman, Phys. Lett. B **359**, 41 (1995); L.M. Johnson and D.W. McKay, Phys. Lett. B **433**, 355 (1998); M. C. Gonzalez-Garcia, Y. Grossman, A. Gusso and Y. Nir, Phys. Rev. D **64**, 096006 (2001); A. M. Gago, M. M. Guzzo, H. Nunokawa, W. J. C. Teves and R. Zukanovich Funchal, Phys. Rev. D **64**, 073003 (2001); A. Datta, R. Gandhi, B. Mukhopadhyaya, and P. Mehta, Phys. Rev. D **64**, 015011 (2001); T. Ota, J. Sato and N. a. Yamashita, Phys. Rev. D **65**, 093015 (2002) M. Campanelli and A. Romanino, Phys. Rev. D **66**, 113001 (2002); P. Huber, T. Schwetz and J. W. F. Valle, Phys. Rev. D **66**, 013006 (2002).
- [32] M. C. Gonzalez-Garcia and C. Pena-Garay, Phys. Rev. D **68**, 093003 (2003)
- [33] A.M. Dziewonski and D.L. Anderson, Phys. Earth Planet. Inter. **25**, 297 (1981).
- [34] M. Maltoni, Nucl. Phys. Proc. Suppl. **114**, 191 (2003); S. Davidson, C. Pena-Garay, N. Rius and A. Santamaria, JHEP **0303**, 011 (2003).
- [35] J. Kameda, Ph.D. thesis, <http://www-sk.icrr.u-tokyo.ac.jp/doc/sk/pub/>.
- [36] M. Ishitsuka, Ph.D. thesis, <http://www-sk.icrr.u-tokyo.ac.jp/doc/sk/pub/>.
- [37] G. L. Fogli, E. Lisi, A. Marrone, D. Montanino and A. Palazzo, Phys. Rev. D **66**, 053010 (2002)
- [38] T. K. Gaisser and M. Honda, Ann. Rev. Nucl. Part. Sci. **52**, 153 (2002)
- [39] M. C. Gonzalez-Garcia, M. Maltoni, C. Pena-Garay and J. W. F. Valle, Phys. Rev. D **63**,

033005 (2001); N. Fornengo, M. C. Gonzalez-Garcia and J. W. Valle, Nucl. Phys. B **580**, 58 (2000); M. C. Gonzalez-Garcia, H. Nunokawa, O. L. Peres and J. W. Valle, Nucl. Phys. B **543**, 3 (1999); M. C. Gonzalez-Garcia, H. Nunokawa, O. L. Peres, T. Stanev and J. W. Valle, Phys. Rev. D **58**, 033004 (1998).